Cell Reports

Article

ApoE4-dependent lysosomal cholesterol accumulation impairs mitochondrial homeostasis and oxidative phosphorylation in human astrocytes

Graphical abstract

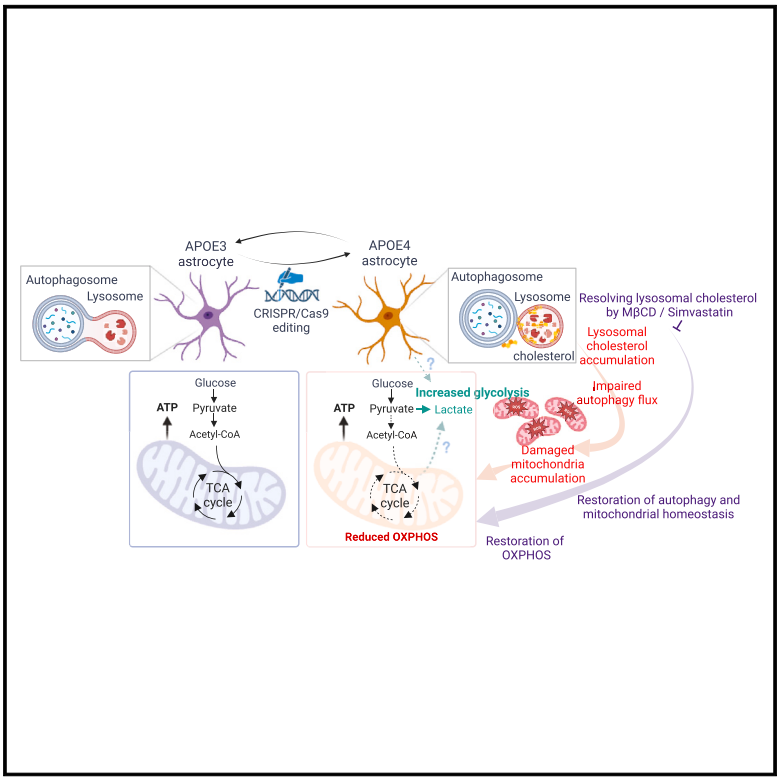

Highlights

- Human ApoE4 astrocytes display increased glycolytic activity and reduced OXPHOS
- ApoE4 induces defective autophagy and mitochondrial dysfunction in human astrocytes
- Mitigating cholesterol burden restores mitochondrial respiration in ApoE4 astrocytes

Authors

Hyein Lee, Sukhee Cho, Mi-Jin Kim, ..., Younghoon Go, In-Kyu Lee, Jinsoo Seo

Correspondence

gotra827@kiom.re.kr (Y.G.), leei@knu.ac.kr (I.-K.L.), jsseo@dgist.ac.kr (J.S.)

In brief

Lee et al. identify ApoE4-dependent mitochondrial dysfunction in human astrocytes and its underlying mechanisms. This study suggests the detrimental effects of ApoE4 on brain metabolism, especially in the later stages of life when the brain greatly depends on oxidative respiration for its function.

Lee et al., 2023, Cell Reports *42*, 113183
October 31, 2023
https://doi.org/10.1016/j.celrep.2023.113183

CellPress

Cell Reports

CellPress
OPEN ACCESS

Article

ApoE4-dependent lysosomal cholesterol accumulation impairs mitochondrial homeostasis and oxidative phosphorylation in human astrocytes

Hyein Lee,[1,9] Sukhee Cho,[1,9] Mi-Jin Kim,[2] Yeo Jin Park,[5,6] Eunji Cho,[7] Yeon Suk Jo,[1,7] Yong-Seok Kim,[1] Jung Yi Lee,[3] Themis Thoudam,[4] Seung-Hwa Woo,[8] Se-In Lee,[1] Juyeong Jeon,[1] Young-Sam Lee,[8] Byung-Chang Suh,[1] Jong Hyuk Yoon,[7] Younghoon Go,[6,*] In-Kyu Lee,[2,3,4,*] and Jinsoo Seo[1,10,*]

[1]Department of Brain Sciences, Daegu Gyeongbuk Institute of Science & Technology, Daegu 42988, South Korea
[2]Department of Internal Medicine, Kyungpook National University School of Medicine, Daegu 41944, South Korea
[3]Leading-Edge Research Center for Drug Discovery and Development for Diabetes and Metabolic Disease, Kyungpook National University School of Medicine, Daegu 41944, South Korea
[4]Research Institute of Aging and Metabolism, Kyungpook National University School of Medicine, Daegu 41944, South Korea
[5]Korean Medicine Life Science, University of Science and Technology, Daejeon 34054, South Korea
[6]Korean Medicine-Application Center, Korea Institute of Oriental Medicine, Daegu 41062, South Korea
[7]Neurodegenerative Disease Research Group, Korea Brain Research Institute, Daegu 41062, South Korea
[8]Department of New Biology, Daegu Gyeongbuk Institute of Science & Technology, Daegu 42988, South Korea
[9]These authors contributed equally
[10]Lead contact
*Correspondence: gotra827@kiom.re.kr (Y.G.), leei@knu.ac.kr (I.-K.L.), jsseo@dgist.ac.kr (J.S.)
https://doi.org/10.1016/j.celrep.2023.113183

SUMMARY

Recent developments in genome sequencing have expanded the knowledge of genetic factors associated with late-onset Alzheimer's disease (AD). Among them, genetic variant ε4 of the *APOE* gene (*APOE4*) confers the greatest disease risk. Dysregulated glucose metabolism is an early pathological feature of AD. Using isogenic ApoE3 and ApoE4 astrocytes derived from human induced pluripotent stem cells, we find that ApoE4 increases glycolytic activity but impairs mitochondrial respiration in astrocytes. Ultrastructural and autophagy flux analyses show that ApoE4-induced cholesterol accumulation impairs lysosome-dependent removal of damaged mitochondria. Acute treatment with cholesterol-depleting agents restores autophagic activity, mitochondrial dynamics, and associated proteomes, and extended treatment rescues mitochondrial respiration in ApoE4 astrocytes. Taken together, our study provides a direct link between ApoE4-induced lysosomal cholesterol accumulation and abnormal oxidative phosphorylation.

INTRODUCTION

Abnormal glucose metabolism is one of the major pathological features of Alzheimer's disease (AD) and is observed in the early phase of disease progression.[1] Apolipoprotein E (ApoE4) is a subtype of apolipoprotein that forms a lipoprotein complex with various lipids, including cholesterol. Of the three isoforms (ε2, ε3, and ε4), ε4 (*APOE4*) is well known as one of the strongest genetic risk factors for AD. Altered brain metabolism, especially increased aerobic glycolysis and impaired oxygen consumption in the brains of ApoE4 carriers, is suggested in studies from human plasma and humanized mouse models.[2–4] However, the causal relationship between ApoE4 and altered glucose metabolism, its underlying mechanisms, and its contribution to AD pathogenesis remains elusive.

Abnormalities in cholesterol homeostasis have gained much attention in ApoE4 research regarding its contribution to the onset of AD. Recent studies on human induced pluripotent stem cells (iPSCs) with the *APOE4* variant showed altered transcriptomic and metabolomic profiles toward the accumulation of cholesterol in glia, such as astrocytes and oligodendrocytes.[5–7] This phenotypic abnormality is especially intriguing because the accumulation of cholesterol in cells disrupts the function of intracellular membranous compartments, including lysosomes, which are important for the homeostasis of mitochondria, essential organelles for energy metabolism.

Here, we asked whether human astrocytes, a major source of ApoE, display altered glucose metabolism in the presence of *APOE4*, and its underlying mechanisms using *APOE4*-carrying AD patient-derived iPSCs and isogenic cells harboring *APOE3* alleles. We found significantly increased glycolysis and reduced mitochondrial respiration in ApoE4 astrocytes. Increased levels of mitochondrial reactive oxygen species (ROS), accumulation of circular mitochondria, and impaired lysosomal activity suggest impaired mitophagy and subsequent accumulation of dysfunctional mitochondria in ApoE4 astrocytes. We further showed that mitigating lysosomal cholesterol accumulation is sufficient to resolve these abnormalities. Together, our study

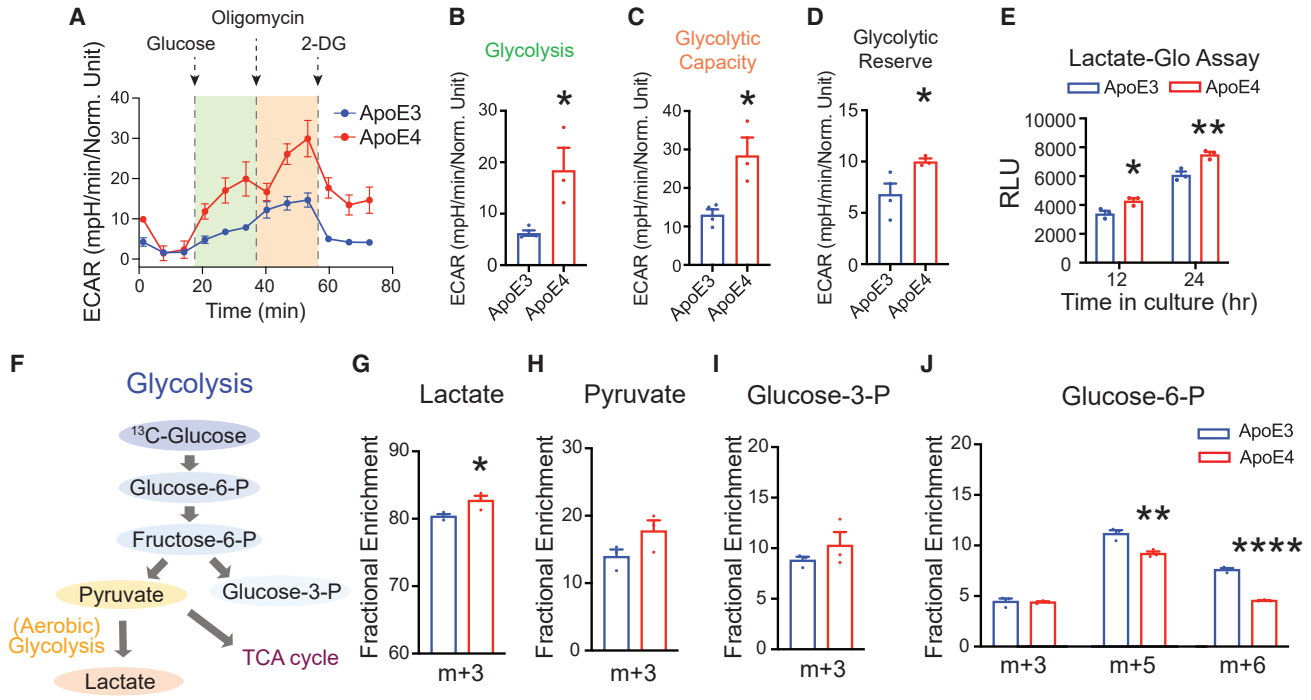

Figure 1. Enhanced aerobic glycolysis in ApoE4 hiPSC-derived astrocytes

(A) Experimental procedure for extracellular acidification rate (ECAR) analysis in ApoE3 and ApoE4 hiPSC-derived astrocytes.

(B–D) Quantifications for glycolysis (B), glycolytic capacity (C), and glycolytic reserve (D) in ApoE3 and ApoE4 astrocytes from 3–4 independent cultures.

(E) Relative light units (RLUs) for Lactate-Glo assay from ApoE3 and ApoE4 astrocyte cultured media harvested for 12 or 24 h. n = 3 independent cultures.

(F) Diagram for using isotope-labeled glucose to measure the metabolic flux.

(G–J) Fractional enrichment for lactate (G), pyruvate (H), glucose-3-phosphate (I), and glucose-6-phosphate (J) was measured by metabolic flux analysis from 3 independent cultures.

*$p < 0.05$, **$p < 0.01$, ****$p < 0.0001$ (Student's t test).

elucidates the impact of ApoE4 on mitochondrial homeostasis and metabolic phenotypes in human astrocytes, which contributes to a better understanding of the pathogenesis of AD.

RESULTS

Generation of isogenic APOE hiPSCs-derived astrocytes

To precisely investigate the effects of ApoE4-induced cholesterol accumulation in human astrocytes, we utilized AD patient-derived iPSCs and isogenic cells, in which the sequence for ApoE4 in the *APOE* gene was converted to ApoE3 by CRISPR-Cas9 genome editing[5] (Figure S1A). These iPSCs were subjected to differentiation into astrocytes, as previously described,[8] followed by fluorescence-activated cell sorting (FACS) based on glutamate-aspartate transporter (GLAST) expression (Figure S1B). The identity of human iPSC (hiPSC)-derived astrocytes was confirmed by immunostaining based on the expression profiles of astrocyte-specific proteins (AQP4, ALDH1L1, S100β, and GFAP) (Figures S1C and S1E). Fetal bovine serum (FBS) was only included in astrocyte culture media to expand cells and was withdrawn at least 4 days before the experiments (Figure S1D). Consistent with previous observations, ApoE4 astrocytes displayed reduced levels of ApoE and impaired Aβ clearance compared with ApoE3 astrocytes[5] (Figures S1F and S1G). These data show the successful generation of human ApoE3 and ApoE4 astrocytes.

Altered glucose metabolism toward enhanced aerobic glycolysis in ApoE4 astrocytes

To determine whether the *APOE4* variant affects glucose metabolic profiles in human astrocytes, we performed a Seahorse metabolic analysis. We first measured the extracellular acidification rate (ECAR) in ApoE3 and ApoE4 hiPSC-derived astrocytes to determine their glycolytic activity. Consistent with previous data from mouse models and humanized mouse cell lines,[4,9] we observed an increase in ECAR upon glucose treatment in ApoE4 astrocytes compared with that in ApoE3 astrocytes, suggesting enhanced glycolysis (Figures 1A and 1B). Glycolytic capacity and glycolytic reserve, measured by sequential treatment with oligomycin and 2-deoxy-D-glucose (2-DG), were also shown to be increased in ApoE4 astrocytes (Figures 1A, 1C, and 1D). An additional bioluminescent assay (Lactate-Glo) was performed to quantify lactate levels by assessing NADH production in the presence of lactate dehydrogenase (LDH), and the results confirmed an increase in lactate release from ApoE4 astrocytes compared with their isogenic cells (Figure 1E). We further investigated the effects of ApoE4 on the metabolic flux in hiPSC-derived astrocytes by tracing ^{13}C-labeled glucose (Figure 1F). We observed an

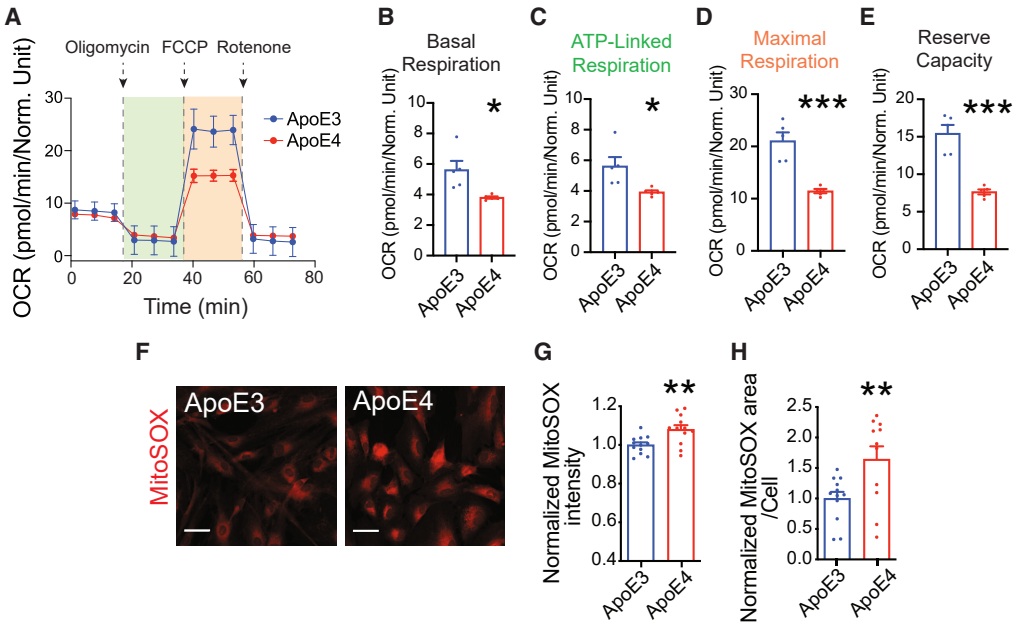

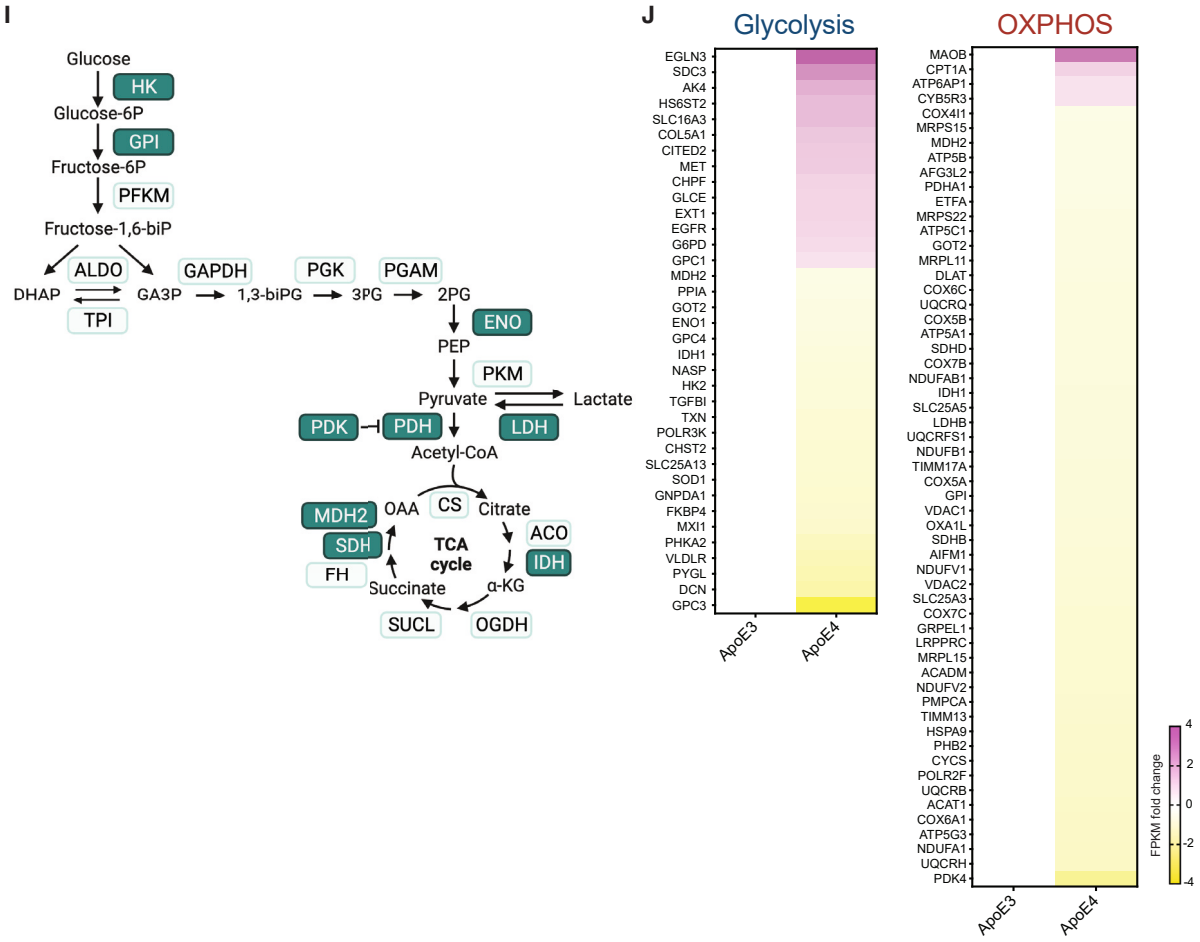

(legend on next page)

increased fraction of m+3 lactate in ApoE4 astrocytes compared with that in ApoE3 astrocytes, indicating enhanced aerobic glycolysis in these cells (Figure 1G). We did not observe any change in the fractions of pyruvate and glycose-3-phosphate between ApoE3 and ApoE4 astrocytes (Figures 1H and 1I), but the m+5 and m+6 fractions of glucose-6-phosphate (Figure 1J) and fructose-6-phosphate (Figure S2A) were significantly reduced in ApoE4 astrocytes, suggesting the possibility of impaired glucose uptake. Although ApoE4 did not show altered fractional enrichment of TCA cycle intermediates, glutamate and aspartate synthesis from the TCA cycle was affected (Figures S2B–S2H). Taken together, these data suggest that ApoE4 alters glucose metabolism toward enhanced aerobic glycolysis.

Impaired mitochondrial respiration with increased ROS in ApoE4 astrocytes

Although aerobic glycolysis is required for acute activity-dependent energy demands in the brain, mitochondrial respiration is a more sustainable and efficient glucose-utilizing energy production process. The oxygen consumption rate assay showed a significantly reduced basal respiration rate in ApoE4 astrocytes compared with that in ApoE3 astrocytes (Figures 2A and 2B). Maximal respiration by FCCP-induced inner mitochondrial membrane depolarization was also decreased in ApoE4 astrocytes, suggesting inefficient energy generation. A significant reduction in ATP-linked respiration indicated that basal respiration was not efficiently coupled with ATP synthesis in ApoE4 astrocytes. The reserve capacity was also significantly reduced in these cells (Figures 2A and 2C–2E). Taken together, these data indicate that ApoE4 impairs mitochondrial oxidative phosphorylation (OXPHOS) in human astrocytes. Mitochondrial dysfunction is often associated with increased mitochondrial ROS levels. Indeed, a higher intensity of MitoSOX signals, indicating an increased level of ROS in mitochondria (Figures 2F–2H), was observed in ApoE4 astrocytes compared with that in isogenic ApoE3 cells. Increased ROS levels induced by ApoE4 were also detected in another isogenic pair derived from a healthy individual with the APOE3 genotype (Figures S3A and S3B). To associate the changes in transcriptome profiles by ApoE4 with glucose metabolic alterations in astrocytes, we analyzed RNA sequencing (RNA-seq) data previously generated from the same cell lines used in this study[5] and determined differential expression patterns of genes related to glycolysis or OXPHOS provided by gene set enrichment analysis (GSEA).[10,11] We found that many genes associated with glycolysis and OXPHOS were regulated by ApoE4 (highlighted in green in Figure 2I). While a relatively equal number of genes involved in glycolysis were being either up- or downregulated, the transcripts of most of the genes associated with OXPHOS were downregulated (Figure 2J). These data suggest the contribution of transcriptional regulation in glucose metabolism in ApoE4 astrocytes.

To validate the ApoE4-dependent elevation in glycolysis and impaired OXPHOS in astrocytes, we subjected KOLF2.1J iPSCs recently claimed as a reference hiPSC line[12] and its isogenic ApoE4 iPSCs generated from the Jackson Laboratory to Seahorse metabolic analysis and MitoSOX staining. Consistently, we observed an ApoE4-dependent increase in glycolytic activity and reduced OXPHOS along with enhanced levels of MitoSOX in this isogenic pair (Figures S4A–S4I).

Impacts of altered glycolytic activity by ApoE4 in astrocytes

We next asked whether altered glycolytic activity by ApoE4 affects stimuli-induced glycolysis in astrocytes using the fluorescence resonance energy transfer (FRET)-based lactate sensor Laconic[13] (Figure S5A). Lactate is known to be produced by glycolysis of astrocytes upon neuronal activation and then transferred to and used by neurons for their high energy requirement. We observed a transient increase in lactate levels in both ApoE3 and ApoE4 astrocytes upon glutamate treatment, which mimics neuronal activation (Figure S5B). Although we did not find the difference in the effect of *APOE* genotype on total levels of lactate synthesis, a statistically significant interaction effect between time and genotypes (two-way ANOVA, time × genotype interaction: $p < 0.05$) was observed due to a relatively sharp transient increase followed by the slow decay of lactate synthesis upon glutamate stimulation in ApoE4 astrocytes (Figure S5C). A recent study reported metabolic reprogramming toward an increase in glycolysis in microglia upon Aβ treatment accompanied by inflammatory responses.[14] We found that Aβ also induces an increase in glycolytic activity in hiPSC-derived astrocytes (Figure S5D). Unlike glutamate treatment, Aβ-induced lactate synthesis tends to increase with time. We did not observe the difference in Aβ-induced lactate synthetic activity in ApoE4 astrocytes compared with in ApoE3 astrocytes and the interaction effect between time and genotypes (Figures S5D and S5E). These data suggest a potential alteration in glycolysis of ApoE4 astrocytes in response to glutamate, the major excitatory neurotransmitter.

Impaired autophagy flux in ApoE4 astrocytes

Damaged mitochondria with increased ROS levels are eliminated through an autophagy-mediated mitochondrial degradation process called mitophagy. The abnormal accumulation of high-ROS mitochondria allowed us to investigate autophagic

Figure 2. Impaired mitochondrial respiration with increased ROS in ApoE4 astrocytes

(A) Experimental procedure for oxygen consumption rate (OCR) analysis in ApoE3 and ApoE4 hiPSC-derived astrocytes.

(B–E) Quantifications for basal respiration (B), ATP-linked respiration (C), maximal respiration (D), and reserve capacity (E) in ApoE3 and ApoE4 astrocytes from 5 independent cultures.

(F) Representative images of MitoSOX assay in ApoE3 or ApoE4 hiPSC-derived astrocytes. n = 11–12 from 3 independent cultures. Scale bar: 20 μm.

(G and H) Quantification of MitoSOX intensity (G) and area (H) in ApoE3 and ApoE4 astrocytes.

(I) Heatmap analysis of relative transcript levels of "glycolysis"- or "OXPHOS"-associated genes. Asterisks represent genes whose expression is significantly altered ($p < 0.05$) in ApoE4 astrocytes compared with those in ApoE3 astrocytes.

(J) Proteins involved in the glucose metabolic process. Highlighted in green are proteins whose transcript expression was affected by ApoE4.

*$p < 0.05$, **$p < 0.01$, ***$p < 0.001$ (Student's t test).

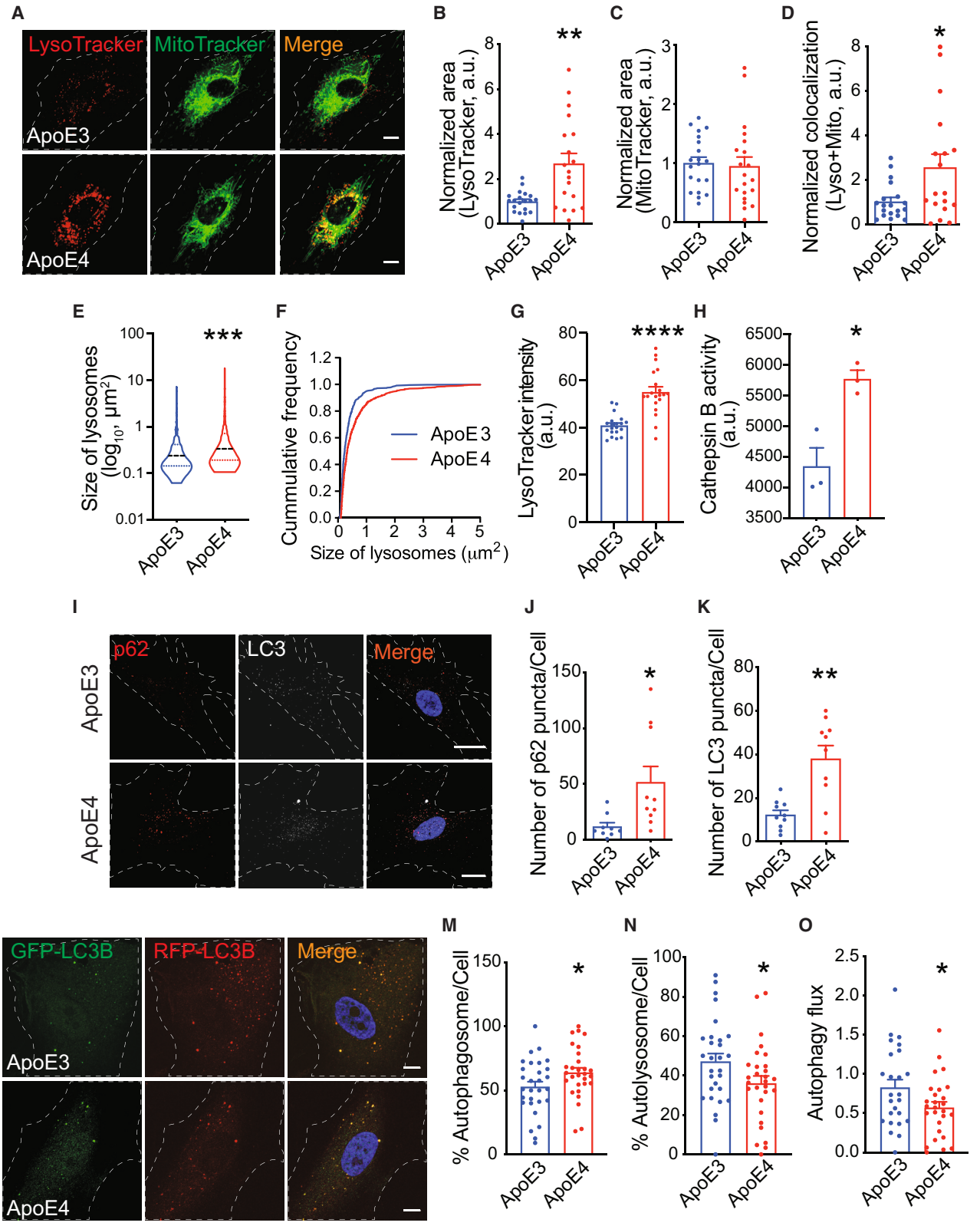

(legend on next page)

activity in ApoE4 astrocytes. First, we examined the colocalization of lysosomes and mitochondria by staining with LysoTracker and MitoTracker. We repeatedly observed an increased lysosomal area, although the mitochondrial area was indistinguishable in ApoE4 astrocytes compared with ApoE3 cells (Figures 3A–3C). The significantly increased colocalization of lysosomes and mitochondria found in ApoE4 astrocytes was likely due to lysosomal dysfunction, suggesting impaired lysosome-dependent mitochondrial degradation in these cells (Figures 3A and 3D). To further address whether ApoE4 induces lysosomal abnormalities in hiPSC-derived astrocytes, we measured the size and activity of lysosomes in ApoE3 and ApoE4 hiPSC-derived astrocytes. We observed an increase in the size of lysosomes in ApoE4 astrocytes (Figures 3E and 3F). We also observed that ApoE4 increased the intensity of LysoTracker, which is positively associated with lysosomal activity (Figure 3G). To further investigate lysosomal dysregulation, we measured the activity of cathepsin B, a lysosomal protease. Consistent with LysoTracker staining, ApoE4 astrocytes displayed an approximately 50% increase in cathepsin B activity compared with ApoE3 astrocytes (Figure 3H). These data indicated ApoE4-dependent dysregulation of lysosomes in hiPSC-derived astrocytes. We then determined autophagic activity in ApoE3 and ApoE4 hiPSC-derived astrocytes by staining with p62, an autophagy substrate, and LC3, a component of autophagosomes widely used as markers to measure autophagic activity. We observed that both p62 and LC3 levels were significantly increased in ApoE4 astrocytes compared with those in ApoE3 astrocytes (Figures 3I–3K), suggesting abnormal accumulation of autophagosomes (increased LC3 levels) by impaired autolysosomal degradation (increased p62 levels) in ApoE4 astrocytes. RFP-GFP-tandem fluorescent LC3 was expressed in hiPSC-derived astrocytes to directly confirm the altered autophagic activity. We observed increased autophagosomes (RFP and GFP) and decreased autolysosomes (RFP only) in ApoE4 astrocytes compared with ApoE3 astrocytes, indicating impaired autophagy flux (Figures 3L–3O).

ApoE4-dependent lysosomal cholesterol accumulation impairs autophagic activity and mitochondrial homeostasis in human astrocytes

Cholesterol accumulation in lysosomes has been shown to impair lysosomal functions, including autophagy-mediated mitochondrial degradation, in various pathological conditions, including Niemann-Pick disease type C.[15,16] Therefore, we assessed cholesterol accumulation in the lysosomes of ApoE4 hiPSC-derived astrocytes using the autofluorescent cholesterol-binding compound filipin III along with LysoTracker to label lysosomes. As previously reported,[5,17] we found a significant accumulation of cholesterol in ApoE4 astrocytes compared with ApoE3 astrocytes (Figures 4A and 4B), which was predominantly observed in lysosomes (Figures 4A and 4C). We next investigated whether the rescue of lysosomal cholesterol levels could attenuate the autophagic activity deficit. We were able to mitigate lysosomal cholesterol accumulation in ApoE4 hiPSC-derived astrocytes with a 4-day treatment of 100 μM methyl-β-cyclodextrin (MβCD), the cholesterol chelating agent known to be effective in reducing lysosomal cholesterol (Figures 4D and 4E).[18,19] MβCD-treated ApoE4 astrocytes also displayed a reduced LysoTracker area in cells comparable to that in ApoE3 astrocytes without disrupting the integrity of the lipids on the plasma membrane measured by time-of-flight secondary ion mass spectrometry (ToF-SIMS) (Figures S6B–S6E). We further observed restoration of lysosomal activity, as indicated by the mitigated intensity of LysoTracker after lysosomal cholesterol depletion (Figures 4D and 4F). Simvastatin treatment also normalized ApoE4-dependent increases in lysosomal cholesterol accumulation and LysoTracker-positive areas in astrocytes (Figures 4G–4I). We then determined the autophagy flux of ApoE4 astrocytes treated with MβCD. We observed the restoration of autolysosomes and autophagosome areas in ApoE4 astrocytes with MβCD treatment, suggesting normalized autophagy flux (Figures 5A–5D). To further confirm this observation, we utilized another ApoE3/ApoE4 isogenic astrocytes. As shown in Figures 3L–3O, ApoE4 astrocytes displayed impaired autophagy flux compared with their isogenic ApoE3 cells, and this effect was attenuated by MβCD treatment (Figures S6F–S6I). To determine whether impaired autophagic activity alters mitochondrial homeostasis in ApoE4 astrocytes, we performed electron microscopy for ultrastructural analysis of the mitochondria (Figure 5E). We were able to determine that the area of individual mitochondria was significantly increased in ApoE4 astrocytes (Figure 5F). Furthermore, mitochondria in ApoE4 astrocytes were more circular and less complex, although there was no difference in perimeter compared with those in ApoE3 astrocytes (Figures 5G–5J). We then examined the effect of cholesterol

Figure 3. Lysosomal dysfunction and impaired autophagic activity in ApoE4 astrocytes

(A) Representative images of LysoTracker and MitoTracker staining in ApoE3 or ApoE4 hiPSC-derived astrocytes. n = 20 from 3 independent cultures. The dashed lines indicate the border of cells. Scale bar: 10 μm.

(B–D) Quantification of area for LysoTracker (B), MitoTracker (C), and colocalization between LysoTracker and MitoTracker (D) in ApoE3 and ApoE4 astrocytes. n = 18–20 from 3 independent cultures.

(E–G) Size of the lysosomes (E), cumulative frequency (F), and mean intensity of signals (G) for ApoE3 and ApoE4 were quantified from LysoTracker staining.

(H) The RFUs in cathepsin B activity assay from ApoE3 and ApoE4 astrocytes. n = 3 independent cultures.

(I) Representative images of p62 and LC3 immunostaining in ApoE3 or ApoE4 hiPSC-derived astrocytes. n = 9–10 from 3 independent cultures. The dashed lines indicate the border of cells. Scale bar: 10 μm.

(J and K) Quantification of the number for p62 puncta (J) and LC3 puncta (K) in ApoE3 or ApoE4 hiPSC-derived astrocytes.

(L) Representative images of RFP-GFP-tandem fluorescent LC3-transfected ApoE3 and ApoE4 astrocytes. n = 29 from 3 independent cultures. The dashed lines indicate the border of cells. Scale bar: 5 μm.

(M–O) Quantification of area for autophagosome (both RFP- and GFP-positive; M), autolysosome (RFP only; N), and the rate of autophagy flux calculated by RFP only/RFP-GFP double positive (O).

*p < 0.05, **p < 0.01, ***p < 0.001, ****p < 0.0001 (Student's t test).

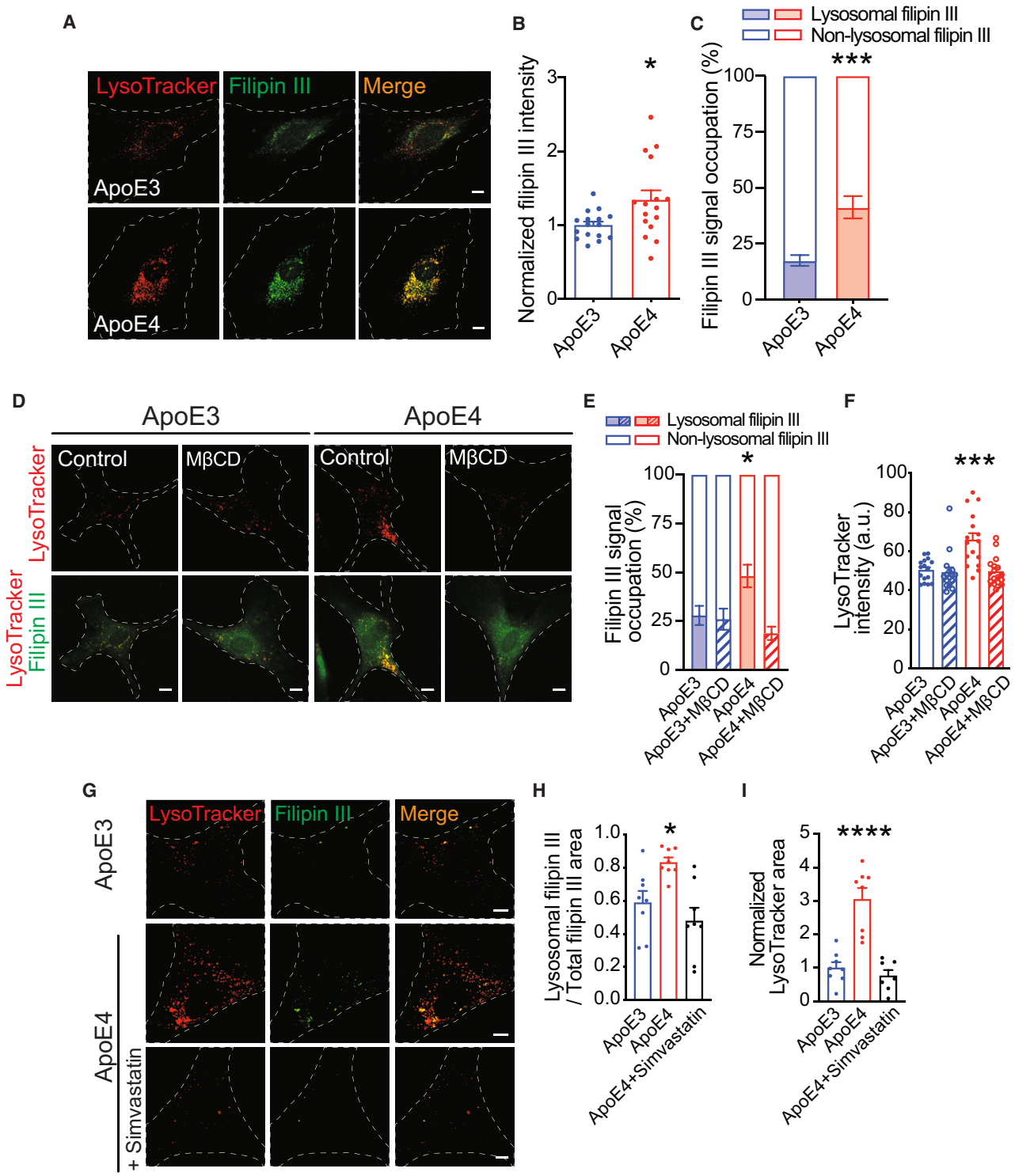

Figure 4. ApoE4-dependent lysosomal cholesterol accumulation impairs autophagic activity and mitochondrial homeostasis in human astrocytes

(A) Representative images of LysoTracker and filipin III staining in ApoE3 or ApoE4 hiPSC-derived astrocytes. n = 16 from 3 independent cultures. The dashed lines indicate the border of cells. Scale bar: 5 μm.

(B and C) Quantification of filipin III intensity (B) and enrichment of filipin III signals in the lysosomes (C) of ApoE3 or ApoE4 hiPSC-derived astrocytes.

(legend continued on next page)

depletion by MβCD on the mitochondrial structure of ApoE4 hiPSC-derived astrocytes. All mitochondrial structural abnormalities observed in ApoE4 astrocytes were completely restored by MβCD treatment (Figures 5E–5J).

Abnormal mitochondrial respiration, but not glycolytic activity, was restored by lysosomal cholesterol depletion in ApoE4 astrocytes

We then asked whether lysosomal cholesterol depletion and autophagic activity restoration are sufficient to normalize glucose metabolism in ApoE4 astrocytes. We treated ApoE4 astrocytes with MβCD (4 days), and cells were subjected to Seahorse extracellular analysis for ECAR and oxygen consumption rate (OCR) measurement. We found that 4 days of MβCD treatment was insufficient to restore both glycolytic activity and OXPHOS in ApoE4 astrocytes (Figures S6J and S6K). The half-life of mitochondria is known to be a couple of weeks in several cell types,[20–22] although their half-life in astrocytes is unknown. Therefore, we tested whether extended treatment of MβCD is required to restore metabolic abnormalities in ApoE4 astrocytes. Indeed, we observed that 14 days of MβCD treatment restored mitochondrial respiration. However, the extended treatment failed to normalize glycolytic activity in ApoE4 astrocytes (Figures 5K–5O), suggesting that ApoE4-induced enhancement of glycolytic activity might be cholesterol independent.

Proteomic analysis confirmed the effects of cholesterol accumulation on mitophagy activity in ApoE4 astrocytes

To determine the impact of cholesterol mitigation in ApoE4 astrocytes on proteome levels, we performed proteomic analysis of ApoE3, ApoE4, and short-term MβCD-treated ApoE4 astrocytes. We found that 254 proteins were downregulated and 238 proteins were upregulated in ApoE4 astrocytes compared with those in ApoE3 astrocytes. Moreover, a statistically significant number of proteins in the list were restored by MβCD treatment (16 out of 254 downregulated, $p = 1.3^{-14}$, 34 out of 238 upregulated, $p = 6.01^{-36}$) (Figure 6A; Table S1). Pathway analysis predicted abnormalities in various signaling pathways in ApoE4 astrocytes. Many of these pathways, including those related to autophagy and protein degradation, were normalized by MβCD treatment (Figure 6B). But consistent with the Seahourse analysis (Figures S6J and S6K), an alteration in glucose metabolism-associated pathways was not restored by short-term MβCD treatment (Figure S6L). The analysis of differentially expressed proteins further confirmed the rescue of a subset of proteins related to "mitophagy" and "metabolic pathways" (Figure 6D).

DISCUSSION

In this study, we found that ApoE4, which greatly increases the risk of AD and lowers the age of onset, leads to abnormal glucose metabolism toward enhanced glycolysis and reduces mitochondrial respiration in human astrocytes. ApoE4 astrocytes display lysosomal dysfunction and impaired autophagic activity, leading to the accumulation of damaged and high-ROS mitochondria. Several previous studies reported[4,9,23] altered glucose metabolism, dysregulated lipid homeostasis, and lysosomal/autophagosomal impairments by ApoE4 in various cell types, including neurons and astrocytes. However, none of these studies attempted to provide the causality among these pathological features and to restore the defects by ApoE4, especially in human astrocytes. Here, by mitigating the intracellular accumulation of cholesterol, especially in lysosomes, we restore autophagic activity and mitochondrial homeostasis in ApoE4 astrocytes. Thus, we provide strong evidence associating cholesterol dysregulation and autophagic defects causing the accumulation of dysfunctional mitochondria in astrocytes by ApoE4.

In the human brain, aerobic glycolysis is associated with the neuronal developmental stage, which gradually decreases with age, whereas glucose usage for mitochondrial OXPHOS is relatively sustained.[24] Thus, the detrimental effects of impaired mitochondrial respiration in ApoE4 astrocytes could be magnified in the later stages of life when the transition of metabolic dependency of the brain from aerobic glycolysis to mitochondrial respiration occurs. This transition can trigger the development of pathology by ApoE4 in astrocytes due to impaired mitochondrial function, limited metabolic supply, and accumulation of oxidative stress. Indeed, human studies have shown that impaired cognitive performance in ApoE4 carriers is prominent after middle age.[25,26] Pathological changes in AD brains precede the onset of clinical symptoms, and one of the first alterations, along with Aβ accumulation, is dysfunctional glucose metabolism.[1,27,28] Therefore, understanding how brain metabolism becomes dysfunctional in AD pathogenesis will open a window of opportunity for drug targeting and early diagnosis, and our data identify a possible contribution of ApoE4 to this process.

Accumulating data suggest an association between glycolysis and AD. Lactate levels in the interstitial fluid were higher in patients than those in unaffected individuals.[29] Proteomics of AD brains revealed strong upregulation of glial proteins associated with glucose metabolism.[30] Further studies are needed to determine the effect of upregulated aerobic glycolysis on the onset of AD and whether it precedes other AD-related pathologies. Increased levels of lactate have also been shown to be

(D) Representative images of LysoTracker and filipin III staining in ApoE3 or ApoE4 hiPSC-derived astrocytes with or without MβCD treatment. n = 16 from 3 independent cultures. The dashed lines indicate the border of cells. Scale bar: 5 μm.
(E and F) Quantification of filipin III enrichment in the lysosomes (E) and LysoTracker intensity (F) of ApoE3 or ApoE4 hiPSC-derived astrocytes with or without MβCD treatment.
(G) Representative images of LysoTracker and filipin III staining in ApoE3 or ApoE4 hiPSC-derived astrocytes with or without simvastatin treatment. n = 8 from 3 independent cultures. The dashed lines indicate the border of cells. Scale bar: 5 μm.
(H and I) Quantification of filipin III enrichment in the lysosomes (H) and LysoTracker area (I) of ApoE3 or ApoE4 hiPSC-derived astrocytes with or without simvastatin treatment.
*$p < 0.05$, ***$p < 0.001$ (ANOVA test followed by Dunnett's post hoc analysis).

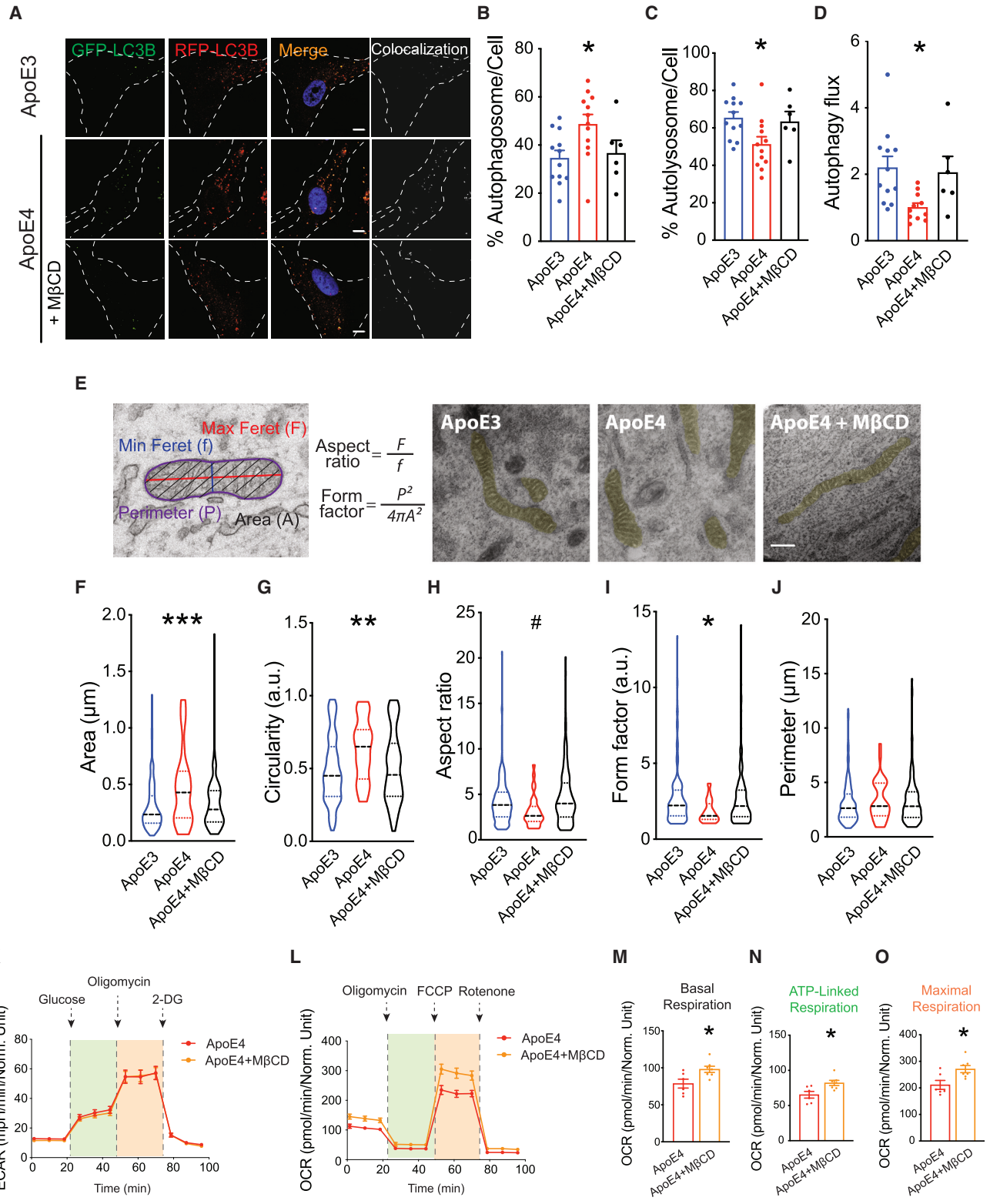

Figure 5. Mitigating lysosomal cholesterol accumulation restores autophagy flux and mitochondrial abnormality in ApoE4 hiPSC-derived astrocytes

(A) Representative images of RFP-GFP-tandem fluorescent LC3-transfected ApoE3, ApoE4, and MβCD-treated ApoE4 astrocytes. n = 6–12 from 2–3 independent cultures. The dashed lines indicate the border of cells. Scale bar: 5 μm.

(legend continued on next page)

correlated with neuronal network activity, as the astrocyte-neuron lactate shuttle is known to regulate neuronal activity.[31] High lactate levels were detected in the brain area, the so-called default network, a set of brain areas spontaneously coactivated across time in the resting state, and showed a strong correlation with the Aβ deposit area in AD brains.[32,33] Young ApoE4 carriers showed increased brain activity in default network regions, as well as in the hippocampus and the temporal lobe, possibly due to increased aerobic glycolysis.[34,35] It is also important to note that increased acidification was shown to trigger Aβ aggregation,[36] suggesting an additional contribution of extracellular acidification by enhanced glycolytic activity in ApoE4 astrocytes to Aβ accumulation in the brain.

By measuring lactate synthesis in real time using the FRET-based lactate sensor Laconic, we provide evidence that ApoE4 may impair the physiological functions of astrocytes, especially those associated with glycolytic activity. Astrocytes transport lactate to neurons, and it is converted to pyruvate and subsequently oxidized to produce energy in response to neuronal activity. Inhibition of astrocyte-specific glycolysis or astrocyte-neuron lactate shuttles was shown to impair long-term memory formation in mice.[37] Another study reported that inhibiting lactate transfer from astrocytes to neurons abolished hippocampal and cortical synaptic plasticity under stress conditions in mice.[38] As we observed a slow decay of glutamate-induced lactate synthesis in ApoE4 astrocytes, further studies are required to determine whether activity-induced lactate supply to neurons and associated cognitive behavior are affected by ApoE4 astrocytes *in vivo*. Similar to previous observations in microglia,[14] we found that Aβ also induces lactate synthesis in astrocytes. As increased glycolytic activity in microglia upon Aβ stimulation was shown to be associated with their inflammatory functions, it would be necessary to address whether increased Aβ-dependent lactate synthesis by ApoE4 alters immune response in astrocytes.

Taken together, our study demonstrating the detrimental effects of astrocyte ApoE4 in glucose metabolism and mitochondria fitness suggests contributions of ApoE4 in AD pathogenesis and provides an explanation of the impact of ApoE4 on later stages of life.

Limitations of the study

First, as including serum in astrocyte culture media is critical for the proliferation of cells after differentiation from hiPSCs, we cultured cells in the presence of serum. Before each experiment, astrocytes were serum deprived for 4 days to minimize the undesirable effect on cells. Although every batch of hiPSC-derived astrocytes was subjected to the validation of their resting state by the treatment of immune stimuli such as polyinosinic-polycytidylic acid after serum deprivation, it is still possible that early exposure of astrocytes to serum induces the changes in the transcriptome, morphology, and function compared with those from cells that never encountered serum. Second, by mitigating cholesterol accumulation, we could rescue autophagic activity and resolve abnormal accumulation of dysfunctional mitochondria in ApoE4 astrocytes; however, enhanced glycolytic activity was not fully restored even after long-term restoration of lysosomal cholesterol accumulation in ApoE4 astrocytes (Figure 5K). Increased cholesterol levels can be caused by enhanced glycolysis and the subsequent synthesis of acetyl-CoA, a source of cholesterol synthesis,[39] which could lead to lysosomal dysfunction and impaired mitochondrial homeostasis (Figure 5K). Whether ApoE4-induced enhancement in glycolytic activity precedes and leads to cholesterol accumulation or whether this abnormality is cholesterol independent is to be addressed by future studies. Lastly, although this study suggests that cholesterol-dependent mitophagy impairment causes mitochondrial dysfunction, it is possible that other adverse effects of disrupted lysosomal function by cholesterol could indirectly lead to mitochondrial dysfunction. Finally, while increased circular forms of mitochondria in ApoE4 astrocytes observed by electron microscopy suggested accumulation of dysfunctional mitochondria, it did not provide direct evidence of ApoE4-induced perturbation of mitochondrial biogenesis or turnover and its causal relationship with metabolic abnormality.

STAR★METHODS

Detailed methods are provided in the online version of this paper and include the following:

- KEY RESOURCES TABLE
- RESOURCE AVAILABILITY
  - Lead contact
  - Materials availability
  - Data and code availability
- EXPERIMENTAL MODEL AND STUDY PARTICIPANT DETAILS
  - iPSCs lines
- METHOD DETAILS
  - Astrocyte differentiation from iPSCs
  - Immunocytochemistry
  - Aβ clearance assay
  - Seahorse extracellular analysis
  - Lactate-glo assay

(B–D) Quantification of area for autophagosome (both RFP- and GFP-positive; B), autolysosome (RFP only; C), and the rate of autophagy flux calculated by RFP only/RFP-GFP double positive (D).
(E) Morphometric description for mitochondria analysis. Mitochondria are marked in yellow in electron microscopy images from ApoE3, ApoE4, and MβCD-treated ApoE4 astrocytes.
(F–I) Quantifications for the area (F), circularity (G), aspect ratio (H), form factor (I), and perimeter (J) of mitochondria in ApoE3, ApoE4, and MβCD-treated ApoE4 astrocytes.
(K and L) Experimental procedure for ECAR (K) and OCR (L) analyses in ApoE4 and MβCD-treated (for 14 days) ApoE4 astrocytes.
(M–O) Quantifications for basal respiration (M), ATP-linked respiration (N), and maximal respiration (O) in ApoE4 and MβCD-treated ApoE4 astrocytes from 6–7 independent cultures.
#$p < 0.06$, *$p < 0.05$, **$p < 0.01$, ***$p < 0.001$ (Student's t test or ANOVA test followed by Dunnett's post hoc analysis).

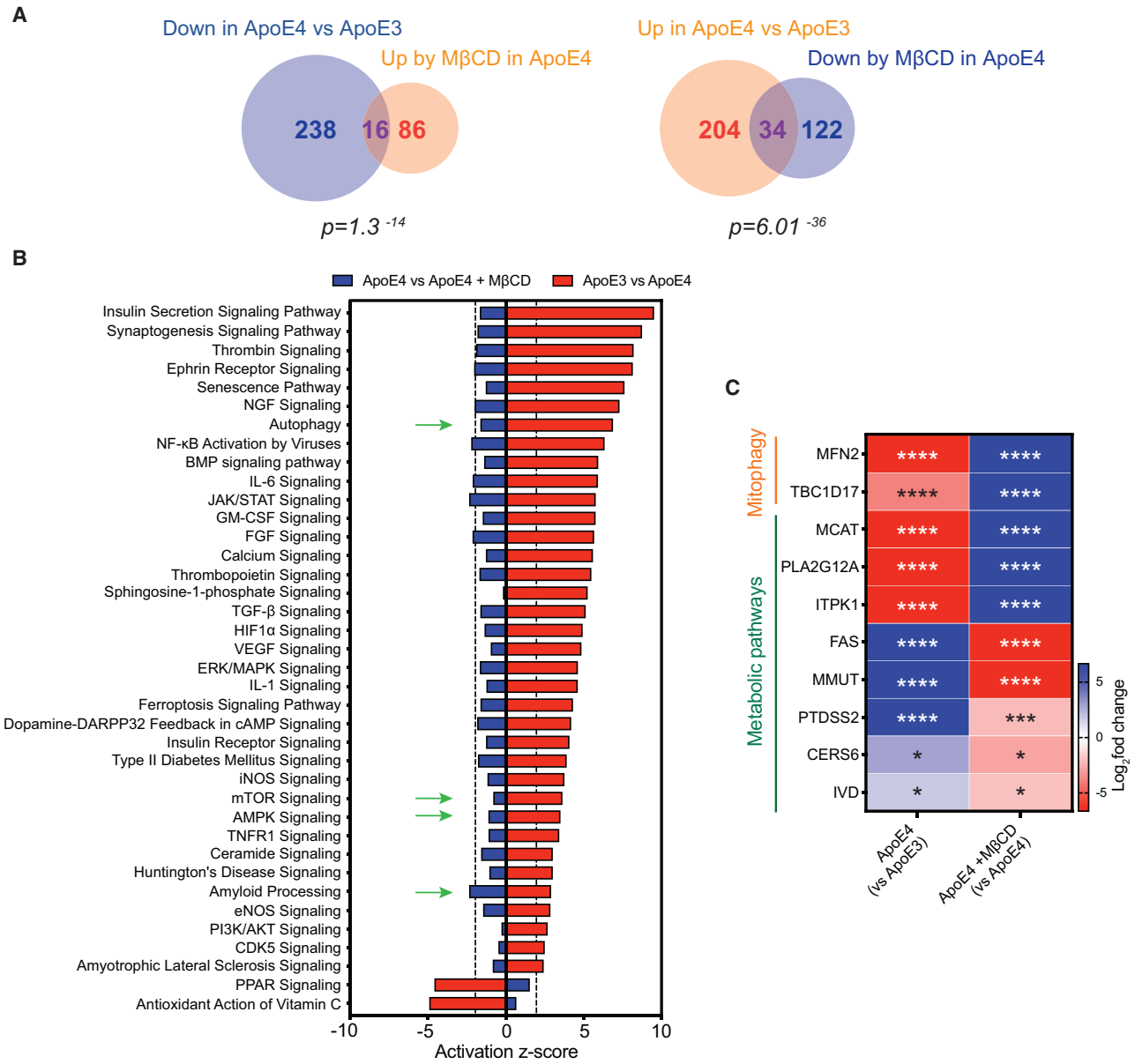

Figure 6. Proteomic analysis confirmed the effects of cholesterol accumulation on mitophagy activity in ApoE4 astrocytes

(A) Venn diagram showing the number of differentially expressed proteins ApoE4 vs. ApoE3 or MβCD-treated ApoE4 vs. ApoE4 astrocytes in the opposite direction. The intersection represents the number of overlapping proteins between two groups, and statistical information is provided.

(B) Selected lists of canonical pathways affected by ApoE4 and partially rescued by MβCD treatment. The dashed lines indicate an activation *Z* score of 1.96 (p = 0.05), and the green arrows point to regulatory pathways related to autophagy.

(C) Heatmap of log_2 fold change values for differentially expressed proteins between ApoE3 vs. ApoE4 or MβCD-treated ApoE4 vs. ApoE4 astrocytes.

11 out of 50 overlapping proteins (A) are related to mitophagy or metabolic pathways from KEGG pathway entries. *p < 0.05, **p < 0.01, ***p < 0.001, ****p < 0.0001 (Student's t test).

- ○ Metabolic flux analysis
- ○ MitoSOX staining
- ○ RNA-seq data analysis
- ○ Förster resonance energy transfer (FRET)-based laconic activity measurement
- ○ Staining of live cell fluorescent organelle dyes
- ○ Filipin III staining
- ○ Autophagy flux assay
- ○ Lysosomal activity assay (cathepsin B)
- ○ Time-of-flight secondary ion mass spectrometry (ToF-SIMS)
- ○ Electron microscopy
- ○ Proteomics
- ● QUANTIFICATION AND STATISTICAL ANALYSIS

SUPPLEMENTAL INFORMATION

Supplemental information can be found online at https://doi.org/10.1016/j.celrep.2023.113183.

ACKNOWLEDGMENTS

The authors would like to thank all members of the Seo lab for their advice and discussion. We also thank Dr. Tsai at MIT and Dr. Yankner at Harvard Medical School for sharing their iPSCs lines. This work was supported by the Korea Brain Research Institute (KBRI) basic research program through KBRI funded by the Ministry of Science and ICT of Korea (MSIT) (22-BR-02-03) to J.H.Y.; the Korea Institute of Oriental Medicine (KIOM) funded by MSIT (KSN2022230) to Y.G.; the National Research Foundation of Korea (NRF) grants funded by MSIT (2022R1A2B5B03001929) to I.-K.L.; and NRF grants (2018M3C7A1056275), the Korea Health Technology R&D Project through the Korea Health Industry Development Institute funded by the Ministry of Health and Welfare (HU21C0111), the KBRI basic research program (21-BR-03-02), and R&D programs of the Daegu Gyeongbuk Institute of Science & Technology (DGIST) (22-CoE-BT-01) funded by MSIT to J.S. The illustrations were created with BioRender.com.

AUTHOR CONTRIBUTIONS

H.L., S.C., Y.G., I.-K.L., and J.S. designed the research; H.L., S.C., M.-J.K., Y.J.P., E.C., Y.S.J., Y.-S.K., J.Y.L., T.T., S.-H.W., S.-I.L., and J.J. performed research; Y.-S.L., B.-C.S., and J.H.Y. contributed new reagents and analytic tools; H.L., S.C., M.-J.K., Y.-S.K., J.Y.L., S.-H.W., S.-I.L., Y.-S.L., B.-C.S., J.H.Y., Y.G., I.-K.L., and J.S. analyzed data; and H.L., S.C., and J.S. wrote the manuscript.

DECLARATION OF INTERESTS

The authors declare no competing interests.

INCLUSION AND DIVERSITY

We support inclusive, diverse, and equitable conduct of research.

Received: November 15, 2022
Revised: August 7, 2023
Accepted: September 13, 2023
Published: September 29, 2023

REFERENCES

1. Gordon, B.A., Blazey, T.M., Su, Y., Hari-Raj, A., Dincer, A., Flores, S., Christensen, J., McDade, E., Wang, G., Xiong, C., et al. (2018). Spatial patterns of neuroimaging biomarker change in individuals from families with autosomal dominant Alzheimer disease: a longitudinal study. Lancet Neurol. *17*, 241–250. https://doi.org/10.1016/s1474-4422(18)30028-0.
2. Ercoli, L., Siddarth, P., Huang, S.-C., Miller, K., Bookheimer, S.Y., Wright, B.C., Phelps, M.E., and Small, G. (2006). Perceived Loss of Memory Ability and Cerebral Metabolic Decline in Persons With the Apolipoprotein E-IV Genetic Risk for Alzheimer Disease. Arch Gen Psychiat *63*, 442–448. https://doi.org/10.1001/archpsyc.63.4.442.
3. Cho, S., Lee, H., and Seo, J. (2021). Impact of Genetic Risk Factors for Alzheimer's Disease on Brain Glucose Metabolism. Mol. Neurobiol. *58*, 2608–2619. https://doi.org/10.1007/s12035-021-02297-x.
4. Farmer, B.C., Williams, H.C., Devanney, N.A., Piron, M.A., Nation, G.K., Carter, D.J., Walsh, A.E., Khanal, R., Young, L.E.A., Kluemper, J.C., et al. (2021). APOE4 lowers energy expenditure in females and impairs glucose oxidation by increasing flux through aerobic glycolysis. Mol. Neurodegener. *16*, 62. https://doi.org/10.1186/s13024-021-00483-y.
5. Lin, Y.-T., Seo, J., Gao, F., Feldman, H.M., Wen, H.-L., Penney, J., Cam, H.P., Gjoneska, E., Raja, W.K., Cheng, J., et al. (2018). APOE4 Causes Widespread Molecular and Cellular Alterations Associated with Alzheimer's Disease Phenotypes in Human iPSC-Derived Brain Cell Types. Neuron *98*, 1141–1154.e7. https://doi.org/10.1016/j.neuron.2018.05.008.
6. Victor, M.B., Leary, N., Luna, X., Meharena, H.S., Scannail, A.N., Bozzelli, P.L., Samaan, G., Murdock, M.H., von Maydell, D., Effenberger, A.H., et al. (2022). Lipid accumulation induced by APOE4 impairs microglial surveillance of neuronal-network activity. Cell Stem Cell *29*, 1197–1212.e8. https://doi.org/10.1016/j.stem.2022.07.005.
7. TCW, J., Qian, L., Pipalia, N.H., Chao, M.J., Liang, S.A., Shi, Y., Jain, B.R., Bertelsen, S.E., Kapoor, M., Marcora, E., et al. (2022). Cholesterol and matrisome pathways dysregulated in astrocytes and microglia. Cell *185*, 2213–2233.e25. https://doi.org/10.1016/j.cell.2022.05.017.
8. TCW, J., Wang, M., Pimenova, A.A., Bowles, K.R., Hartley, B.J., Lacin, E., Machlovi, S.I., Abdelaal, R., Karch, C.M., Phatnani, H., et al. (2017). An Efficient Platform for Astrocyte Differentiation from Human Induced Pluripotent Stem Cells. Stem Cell Rep. *9*, 600–614. https://doi.org/10.1016/j.stemcr.2017.06.018.
9. Qi, G., Mi, Y., Shi, X., Gu, H., Brinton, R.D., and Yin, F. (2021). ApoE4 Impairs Neuron-Astrocyte Coupling of Fatty Acid Metabolism. Cell Rep. *34*, 108572. https://doi.org/10.1016/j.celrep.2020.108572.
10. Subramanian, A., Tamayo, P., Mootha, V.K., Mukherjee, S., Ebert, B.L., Gillette, M.A., Paulovich, A., Pomeroy, S.L., Golub, T.R., Lander, E.S., and Mesirov, J.P. (2005). Gene set enrichment analysis: A knowledge-based approach for interpreting genome-wide expression profiles. Proc. Natl. Acad. Sci. USA. *102*, 15545–15550. https://doi.org/10.1073/pnas.0506580102.
11. Mootha, V.K., Lindgren, C.M., Eriksson, K.-F., Subramanian, A., Sihag, S., Lehar, J., Puigserver, P., Carlsson, E., Ridderstråle, M., Laurila, E., et al. (2003). PGC-1α-responsive genes involved in oxidative phosphorylation are coordinately downregulated in human diabetes. Nat. Genet. *34*, 267–273. https://doi.org/10.1038/ng1180.
12. Pantazis, C.B., Yang, A., Lara, E., McDonough, J.A., Blauwendraat, C., Peng, L., Oguro, H., Kanaujiya, J., Zou, J., Sebesta, D., et al. (2022). A reference human induced pluripotent stem cell line for large-scale collaborative studies. Cell Stem Cell *29*, 1685–1702.e22. https://doi.org/10.1016/j.stem.2022.11.004.
13. San Martín, A., Ceballo, S., Ruminot, I., Lerchundi, R., Frommer, W.B., and Barros, L.F. (2013). A Genetically Encoded FRET Lactate Sensor and Its Use To Detect the Warburg Effect in Single Cancer Cells. PLoS One *8*, e57712. https://doi.org/10.1371/journal.pone.0057712.
14. Baik, S.H., Kang, S., Lee, W., Choi, H., Chung, S., Kim, J.-I., and Mook-Jung, I. (2019). A Breakdown in Metabolic Reprogramming Causes Microglia Dysfunction in Alzheimer's Disease. Cell Metab. *30*, 493–507.e6. https://doi.org/10.1016/j.cmet.2019.06.005.
15. Maetzel, D., Sarkar, S., Wang, H., Abi-Mosleh, L., Xu, P., Cheng, A.W., Gao, Q., Mitalipova, M., and Jaenisch, R. (2014). Genetic and Chemical Correction of Cholesterol Accumulation and Impaired Autophagy in Hepatic and Neural Cells Derived from Niemann-Pick Type C Patient-Specific iPS Cells. Stem Cell Rep. *2*, 866–880. https://doi.org/10.1016/j.stemcr.2014.03.014.
16. Davis, O.B., Shin, H.R., Lim, C.-Y., Wu, E.Y., Kukurugya, M., Maher, C.F., Perera, R.M., Ordonez, M.P., and Zoncu, R. (2021). NPC1-mTORC1 Signaling Couples Cholesterol Sensing to Organelle Homeostasis and Is a Targetable Pathway in Niemann-Pick Type C. Dev. Cell *56*, 260–276.e7. https://doi.org/10.1016/j.devcel.2020.11.016.
17. Lee, S.-I., Jeong, W., Lim, H., Cho, S., Lee, H., Jang, Y., Cho, J., Bae, S., Lin, Y.-T., Tsai, L.-H., et al. (2021). APOE4-carrying human astrocytes oversupply cholesterol to promote neuronal lipid raft expansion and Aβ generation. Stem Cell Rep. *16*, 2128–2137. https://doi.org/10.1016/j.stemcr.2021.07.017.
18. Li, R., Hao, J., Fujiwara, H., Xu, M., Yang, S., Dai, S., Long, Y., Swaroop, M., Li, C., Vu, M., et al. (2017). Analytical Characterization of Methyl-β-Cyclodextrin for Pharmacological Activity to Reduce Lysosomal

Cholesterol Accumulation in Niemann-Pick Disease Type C1 Cells. Assay Drug Dev. Technol. *15*, 154–166. https://doi.org/10.1089/adt.2017.774.

19. Swaroop, M., Thorne, N., Rao, M.S., Austin, C.P., McKew, J.C., and Zheng, W. (2012). Evaluation of Cholesterol Reduction Activity of Methyl-β-cyclodextrin Using Differentiated Human Neurons and Astrocytes. J. Biomol. Screen *17*, 1243–1251. https://doi.org/10.1177/1087057112456877.
20. Krishna, S., Arrojo E Drigo, R., Capitanio, J.S., Ramachandra, R., Ellisman, M., and Hetzer, M.W. (2021). Identification of long-lived proteins in the mitochondria reveals increased stability of the electron transport chain. Dev. Cell *56*, 2952–2965.e9. https://doi.org/10.1016/j.devcel.2021.10.008.
21. Facundo, H.d.T.F., Brainard, R.E., Caldas, F.R.d.L., Lucas, A.M.B., and Lucas, A.M.B. (2017). Mitochondria and Cardiac Hypertrophy. Adv. Exp. Med. Biol. *982*, 203–226. https://doi.org/10.1007/978-3-319-55330-6_11.
22. Menzies, R.A., and Gold, P.H. (1971). The Turnover of Mitochondria in a Variety of Tissues of Young Adult and Aged Rats. J. Biol. Chem. *246*, 2425–2429. https://doi.org/10.1016/s0021-9258(18)62305-1.
23. Wu, L., Zhang, X., and Zhao, L. (2018). Human ApoE Isoforms Differentially Modulate Brain Glucose and Ketone Body Metabolism: Implications for Alzheimer's Disease Risk Reduction and Early Intervention. J. Neurosci. *38*, 6665–6681. https://doi.org/10.1523/jneurosci.2262-17.2018.
24. Goyal, M.S., Vlassenko, A.G., Blazey, T.M., Su, Y., Couture, L.E., Durbin, T.J., Bateman, R.J., Benzinger, T.L.S., Morris, J.C., and Raichle, M.E. (2017). Loss of Brain Aerobic Glycolysis in Normal Human Aging. Cell Metab. *26*, 353–360.e3. https://doi.org/10.1016/j.cmet.2017.07.010.
25. Evans, S., Dowell, N.G., Tabet, N., Tofts, P.S., King, S.L., and Rusted, J.M. (2014). Cognitive and neural signatures of the APOE E4 allele in mid-aged adults. NBA *35*, 1615–1623. https://doi.org/10.1016/j.neurobiolaging.2014.01.145.
26. Rawle, M.J., Davis, D., Bendayan, R., Wong, A., Kuh, D., and Richards, M. (2018). Apolipoprotein-E (Apoe) ε4 and cognitive decline over the adult life course. Transl Psychiat *8*, 18. https://doi.org/10.1038/s41398-017-0064-8.
27. Weise, C.M., Chen, K., Chen, Y., Kuang, X., Savage, C.R., and Reiman, E.M.; Alzheimer's Disease Neuroimaging Initiative (2018). Left lateralized cerebral glucose metabolism declines in amyloid-β positive persons with mild cognitive impairment. Neuroimage. Clin. *20*, 286–296. https://doi.org/10.1016/j.nicl.2018.07.016.
28. Croteau, E., Castellano, C.A., Fortier, M., Bocti, C., Fulop, T., Paquet, N., and Cunnane, S.C. (2018). A cross-sectional comparison of brain glucose and ketone metabolism in cognitively healthy older adults, mild cognitive impairment and early Alzheimer's disease. Exp. Gerontol. *107*, 18–26. https://doi.org/10.1016/j.exger.2017.07.004.
29. Carroll, C.M., and Macauley, S.L. (2019). The Interaction Between Sleep and Metabolism in Alzheimer's Disease: Cause or Consequence of Disease? Front. Aging Neurosci. *11*, 258. https://doi.org/10.3389/fnagi.2019.00258.
30. Johnson, L.A. (2020). APOE and metabolic dysfunction in Alzheimer's disease. Int. Rev. Neurobiol. *154*, 131–151. https://doi.org/10.1016/bs.irn.2020.02.002.
31. Suzuki, A., Stern, S.A., Bozdagi, O., Huntley, G.W., Walker, R.H., Magistretti, P.J., and Alberini, C.M. (2011). Astrocyte-neuron lactate transport is required for long-term memory formation. Cell *144*, 810–823. https://doi.org/10.1016/j.cell.2011.02.018.
32. Buckner, R.L., Snyder, A.Z., Shannon, B.J., LaRossa, G., Sachs, R., Fotenos, A.F., Sheline, Y.I., Klunk, W.E., Mathis, C.A., Morris, J.C., and Mintun, M.A. (2005). Molecular, Structural, and Functional Characterization of Alzheimer's Disease: Evidence for a Relationship between Default Activity, Amyloid, and Memory. J. Neurosci. *25*, 7709–7717. https://doi.org/10.1523/jneurosci.2177-05.2005.
33. van der Kant, R., Goldstein, L.S.B., and Ossenkoppele, R. (2020). Amyloid-β-independent regulators of tau pathology in Alzheimer disease. Nat. Rev. Neurosci. *21*, 21–35. https://doi.org/10.1038/s41583-019-0240-3.
34. Vlassenko, A.G., Vaishnavi, S.N., Couture, L., Sacco, D., Shannon, B.J., Mach, R.H., Morris, J.C., Raichle, M.E., and Mintun, M.A. (2010). Spatial correlation between brain aerobic glycolysis and amyloid-β (Aβ) deposition. Proc. Natl. Acad. Sci. USA *107*, 17763–17767. https://doi.org/10.1073/pnas.1010461107.
35. Filippini, N., MacIntosh, B.J., Hough, M.G., Goodwin, G.M., Frisoni, G.B., Smith, S.M., Matthews, P.M., Beckmann, C.F., and Mackay, C.E. (2009). Distinct patterns of brain activity in young carriers of the APOE-epsilon4 allele. Proc. Natl. Acad. Sci. USA *106*, 7209–7214. https://doi.org/10.1073/pnas.0811879106.
36. Su, Y., and Chang, P.-T. (2001). Acidic pH promotes the formation of toxic fibrils from β-amyloid peptide. Brain Res. *893*, 287–291. https://doi.org/10.1016/s0006-8993(00)03322-9.
37. Mächler, P., Wyss, M.T., Elsayed, M., Stobart, J., Gutierrez, R., von Faber-Castell, A., Kaelin, V., Zuend, M., San Martín, A., Romero-Gómez, I., et al. (2016). In Vivo Evidence for a Lactate Gradient from Astrocytes to Neurons. Cell Metab. *23*, 94–102. https://doi.org/10.1016/j.cmet.2015.10.010.
38. Murphy-Royal, C., Johnston, A.D., Boyce, A.K.J., Diaz-Castro, B., Institoris, A., Peringod, G., Zhang, O., Stout, R.F., Spray, D.C., Thompson, R.J., et al. (2020). Stress gates an astrocytic energy reservoir to impair synaptic plasticity. Nat. Commun. *11*, 2014. https://doi.org/10.1038/s41467-020-15778-9.
39. Shi, Q., Chen, J., Zou, X., and Tang, X. (2022). Intracellular Cholesterol Synthesis and Transport. Front. Cell Dev. Biol. *10*, 819281. https://doi.org/10.3389/fcell.2022.819281.
40. Meyer, K., Feldman, H.M., Lu, T., Drake, D., Lim, E.T., Ling, K.-H., Bishop, N.A., Pan, Y., Seo, J., Lin, Y.-T., et al. (2019). REST and Neural Gene Network Dysregulation in iPSC Models of Alzheimer's Disease. Cell Rep. *26*, 1112–1127.e9. https://doi.org/10.1016/j.celrep.2019.01.023.
41. Go, Y., Jeong, J.Y., Jeoung, N.H., Jeon, J.-H., Park, B.-Y., Kang, H.-J., Ha, C.-M., Choi, Y.-K., Lee, S.J., Ham, H.J., et al. (2016). Inhibition of Pyruvate Dehydrogenase Kinase 2 Protects Against Hepatic Steatosis Through Modulation of Tricarboxylic Acid Cycle Anaplerosis and Ketogenesis. Diabetes *65*, 2876–2887. https://doi.org/10.2337/db16-0223.
42. Keum, D., Baek, C., Kim, D.-I., Kweon, H.-J., and Suh, B.-C. (2014). Voltage-dependent regulation of CaV2.2 channels by Gq-coupled receptor is facilitated by membrane-localized β subunit. J. Gen. Physiol. *144*, 297–309. https://doi.org/10.1085/jgp.201411245.
43. Cho, S., Lee, H., Jung, M., Hong, K., Woo, S.-H., Lee, Y.-S., Kim, B.J., Jeon, M.Y., Seo, J., and Mun, J.Y. (2021). Neuromyelitis optica (NMO)-IgG-driven organelle reorganization in human iPSC-derived astrocytes. FASEB J, Off. Publ. Fed. Am. Soc. Exp. Biol. *35*, e21894. https://doi.org/10.1096/fj.202100637r.
44. Lim, H., Lee, S.Y., Moon, D.W., and Kim, J.Y. (2019). Preparation of cellular samples using graphene cover and air-plasma treatment for time-of-flight secondary ion mass spectrometry imaging. RSC Adv. *9*, 28432–28438. https://doi.org/10.1039/c9ra05205d.

STAR★METHODS

KEY RESOURCES TABLE

REAGENT or RESOURCE	SOURCE	IDENTIFIER
Antibodies		
Anti-AQP4 antibody	Sigma-Aldrich	Cat#SAB5200112
Anti-ALDH1L1 antibody (YY8)	Santa Cruz Biotechnology	Cat#sc-100497, RRID:AB_2224180
Anti-S100β antibody	Abcam	Cat#ab868, RRID:AB_306716
Anti-GFAP antibody	Abcam	Cat#ab53554, RRID:AB_880202
Anti-ApoE antibody	Abcam	Cat#ab52607, RRID:AB_867704
Anti-p62 antibody	Abcam	Cat#ab56416, RRID:AB_945626
Anti-LC3B antibody	Novus	Cat#NB100-2220, RRID:AB_10003146
Chemicals, peptides, and recombinant proteins		
mTeSR1	STEMCELL Technologies	Cat#85850
hESC-qualified matrigel	Corning	Cat#356277
Astrocyte Medium	ScienCell	Cat#1801
DPBS	Biowest	Cat#L0615-500
Donkey serum	Merck	Cat#S30-100ML
Fluorescence Mounting Medium	DAKO	Cat#S3025
Amyloid-beta (1–42) Human	AnaSpec	Cat#AS-20276-5
AEBSF	Thermo Fisher Scientific	Cat#78431
XFe96 cell culture plate	Agilent Technologies	Cat#4103794-100
XF DMEM medium	Agilent Technologies	Cat#103575-100
Seahorse XF Glucose Solution	Agilent Technologies	Cat#103577-100
Seahorse XF Pyruvate Solution	Agilent Technologies	Cat#103578-100
Seahorse XF Glutamine Solution	Agilent Technologies	Cat#103579-100
Oligomycin	Sigma-Aldrich	Cat#75351
2-Deoxy-D-glucose	Sigma-Aldrich	Cat#8375
FCCP [carbonyl cyanide 4-(trifluoromethoxy)-phenylhydrazone]	Sigma-Aldrich	Cat#C2920
Rotenone	Sigma-Aldrich	Cat#R8875
[U-$^{13}C^{6}$] glucose	Sigma-Aldrich	Cat#660663
MitoSOX	Invitrogen	Cat#M36008
LysoTracker red DND-99	Thermo Fisher Scientific	Cat#L7528
MitoTracker Green FM	Thermo Fisher Scientific	Cat#M7514
ProteaseMAX	Promega	Cat#V2071
Trypsin Lys-C mixture	Promega	Cat#V5071
Trifluoroacetic acid	Thermo Fisher Scientific	Cat#28904
C18 spin column	Thermo Fisher Scientific	Cat#89870
Critical commercial assays		
Amyloid-beta 42 Human ELISA kit	Thermo Fisher Scientific	Cat#KHB3442
Lactate-Glo assay kit	Promega	Cat#J5021
Lysosomal activity assay (Cathepsin B)	BioVision	Cat#K140-100
Cholesterol staining kit (Filipin III)	BioVision	Cat#K587
Deposited data		
RNA-seq data from hiPSC-derived astrocytes	Lin et al.[5]	GEO: GSE102956
Proteome from ApoE3 astrocytes, ApoE4 astrocytes and MβCD-treated ApoE4 astrocytes	In this study	PRIDE repository: PXD045298

(*Continued on next page*)

Continued

REAGENT or RESOURCE	SOURCE	IDENTIFIER
Experimental models: Cell lines		
Human iPSC line from a healthy control (*APOE3*)	Coriell	Cat# AG09173
APOE4 isogenic line from #AG09173	Tsai Laboratory (Lin et al.)[5]	N/A
Human iPSC line from a sAD patient (*APOE4*)	Coriell	Cat# AG10788
APOE3 isogenic line from #AG10788	Tsai Laboratory (Lin et al.)[5]	N/A
Human iPSC line from a healthy control (*APOE3*)	The Jackson Laboratory	Cat#JIPC1000
APOE4 isogenic line from #JIPC1000	The Jackson Laboratory	Cat#JIPC1150
Recombinant DNA		
ptfLC3	Addgene	Cat#21074, RRID:Addgene_21074
Laconic/pcDNA3.1(−)	Addgene	Cat#44238, RRID:Addgene_44238
Software and algorithms		
Proteome Discoverer	Thermo Fisher Scientific	RRID:SCR_014477
Prism 9	GraphPad	RRID:SCR_002798
Seahorse Wave	Agilent Technologies	RRID:SCR_014526
DAVID	LHRI	RRID:SCR_001881

RESOURCE AVAILABILITY

Lead contact

Further requests for the resources and reagents should be directed to and will be fulfilled by the lead contact, Jinsoo Seo (jsseo@dgist.ac.kr).

Materials availability

All unique materials and reagents will be available from the lead contact with a completed materials transfer agreement upon reasonable request.

Data and code availability

- This paper analyzes existing, publicly available RNA-seq data deposited in the Gene Expression Omnibus (GEO) database. The MS proteomics data have been deposited at the ProteomeXchange Consortium via the PRIDE partner repository and are publicly available as of the date of publication. Accession numbers are listed in the Key resources table.
- This paper does not report the original code.
- Any additional information required to reanalyze the data reported in this paper is available from the lead contact upon request.

EXPERIMENTAL MODEL AND STUDY PARTICIPANT DETAILS

iPSCs lines

Three ApoE3 and ApoE4 isogenic iPSCs pairs were used to determine the effect of APOE4 genotype without inter-donor variability.[5,12,40] Specifically, the sporadic AD iPSC carrying the *APOE4* allele was obtained from the Coriell Institute (#AG10788, female, age 87), and the ApoE3 isogenic iPSC line was generated by the CRISPR/Cas9 genome editing [5]. Another isogenic pair was generated from the Coriell Institute's fibroblast line derived from a healthy individual (#AG09173, female, age 75) by Dr. Yankner's Laboratory at Harvard Medical School.[5,40] We also utilized 'a reference hiPSC line (KOLF2.1J_#JIPC1000)' selected by the iPSC Neurodegenerative Disease Initiative (iNDI) from the NIH's Center for Alzheimer's and Related Dementias (CARD) and distributed by the Jackson Laboratory,[12] and isogenic ApoE4 line (#JIPC1150).

METHOD DETAILS

Astrocyte differentiation from iPSCs

iPSCs were cultured on hESC-qualified matrigel (Corning) in mTeSR1 media (Stemcell) until they reached 100% confluence, then differentiated into neural progenitor cells (NPCs) with neural induction media as previously described.[5] After validating the identity of NPCs by immunostaining with anti-SOX-2 and Nestin antibodies, they were further differentiated into astrocytes with Astrocyte Medium (ScienCell) as described previously.[8] Because having FBS in astrocyte culture media was known to make astrocytes

more proliferative, we only included FBS in astrocyte culture media for expanding cells after the differentiation process and withdrew at least 4 days before the experiments.

Immunocytochemistry

Astrocytes were plated on glass coverslips, and experiments were performed after at least 24 h recovery. Cells were rinsed three times with DPBS and incubated in 4% paraformaldehyde for 10 min for fixation. Following washing three times with DPBS, astrocytes were incubated with a blocking solution (0.1% Triton X-100, 10% donkey serum, 2% BSA, and 1M glycine in PBS) for 1 h at room temperature. Primary antibodies were diluted in a blocking solution to incubate for 1–2 h at room temperature. After washing cells three times with 0.1% Triton X-100 in DPBS for 5 min, appropriate secondary antibodies that are conjugated with fluorophore were diluted in a blocking solution and incubated for 1 h at room temperature. Coverslips were mounted with DAKO mounting media (Agilent) after washing three times with 0.1% Triton X-100 in DBPS. Images were acquired with the LSM 800 confocal microscope (Zeiss).

Aβ clearance assay

Astrocytes were seeded on 96-well plates at a density of 1×10^4 cells/well. The day after plating cells, the medium was replaced with a fresh medium containing 250 ng/mL oligomeric amyloid-beta 1–42 (AnaSpec) in each well (including an empty well as a control one). Following incubation for 48 h, the medium was collected, and AEBSF was added to each sample to stabilize Aβ at a final concentration of 1 mM. $A\beta_{42}$ levels in the medium were analyzed using an Amyloid-beta 42 Human ELISA kit (Invitrogen) according to the manufacturer's instructions. The absorbance of each well was detected with SpectroMax plus 384 (Molecular Devices) at 450 nm wavelength, and the uptake level was calculated by subtracting from the value of blank control.

Seahorse extracellular analysis

Astrocytes were plated on XFe96 cell culture plates (Agilent Technologies) the day before analysis. On the day of the experiment, the media was changed to XF assay medium (XF DMEM medium (Agilent Technologies) supplemented with 10 mM glucose (Agilent Technologies), 1 mM pyruvate (Agilent Technologies), and 2 mM glutamine (Agilent Technologies) for cell mito stress test; XF DMEM medium supplemented with 2mM glutamine for glycolysis stress test) and incubated in a non-CO_2 incubator for 30 min. After preparing reagents for the assay, plates were loaded in the XFe96 Extracellular Flux Analyzer (Agilent Technologies) to measure the extracellular acidification rate (ECAR) and oxygen consumption rate (OCR). Baseline measurements were collected 3 times, and ECAR or OCR was recorded as drugs were injected sequentially [ECAR: glucose (10 mM, Sigma-Aldrich), oligomycin (1 μM, Sigma-Aldrich), 2DG (2-Deoxy-D-glucose) (50 mM, Sigma-Aldrich)], [OCR: oligomycin (1 μM, Sigma-Aldrich), FCCP (carbonyl cyanide 4-(trifluoromethoxy)-phenylhydrazone) (1 μM, Sigma-Aldrich), and rotenone (1 μM, Sigma-Aldrich)]. Glycolytic and OXPHOS parameters were calculated using Seahorse software as described in the following. ECAR: glycolysis = (maximum rate measurement before oligomycin injection) − (last rate measurement before glucose injection), glycolytic capacity = (maximum rate measurement after oligomycin injection) − (last rate measurement before glucose injection), glycolytic reserve = (glycolytic capacity) − (glycolysis); OCR: basal respiration = (last rate measurement before first injection) − (non-mitochondrial respiration rate), maximal respiration = (maximum rate measurement after FCCP injection) − (non-mitochondrial respiration), ATP-linked respiration = (last rate measurement before oligomycin injection) − (minimum rate measurement after oligomycin injection), reserve capacity = (maximal respiration) − (basal respiration). At the end of the experiment, cell number was measured with DAPI staining to normalize the value using ImageXpress Micro Confocal (Molecular Devices).

Lactate-glo assay

To directly measure secreted lactate levels from astrocytes, the Lactate-Glo assay kit (Promega) was used according to the manufacturer's instructions. In brief, astrocytes were seeded at a density of 1×10^4 cells/well in 96-well plates. After changing the medium for fresh, the conditioned media were harvested at each time point and diluted 1:100 in DPBS. Luminescence detection was performed using microplate reader SpectroMax plus 384 (Molecular Devices).

Metabolic flux analysis

Astrocytes were washed glucose-free astrocyte medium (ScienCell). Then they incubated with the tracer, 5.5 mM [U-$^{13}C_6$] glucose (Sigma-Aldrich), astrocyte medium for 4 h. The cells were washed with 3 mL ice-cold 0.9% NaCl twice and then collected in Eppendorf tubes and were resuspended in 200 μL of ice-cold metabolite extraction solution (chloroform:methanol:water 1:3:1, v/v) and then sonicated. After incubation on ice for 30 min, the samples were collected by centrifugation at 13,000 rpm for 20 min. All the samples were lyophilized and re-suspended in 200 μL of water containing 0.1% formic acid prior to LC-MS/MS analysis.[41] All metabolic samples were acquired and analyzed by LCMS-8060 (Shimadzu).

MitoSOX staining

Cells were stained with 5 μM MitoSOX (Invitrogen) for 10 min in an incubator, followed by washing with AM media twice. Live imaging was performed with the LSM 800 confocal microscope.

RNA-seq data analysis

Previously generated RNA-seq data from isogenic astrocytes used in this study[5] were analyzed to compare genes associated with glycolysis or OXPHOS [200 genes for both glycolysis 'HALLMARK_GLYCOLYSIS' and OXPHOS 'HALLMARK_OXIDATIVE PHOSPHORYLATION' based on 'Gene Set Enrichment Analysis' provided by UCSD and the Broad Institute (https://www.gsea-msigbd.org/gsea/index.jsp)] and differential expressed genes between ApoE3 and ApoE4 astrocytes.

Förster resonance energy transfer (FRET)-based laconic activity measurement

Laconic, an FRET-based lactate sensor[13] (Addgene #44238) was transfected 1 day before the analysis. FRET between mTFP and Venus fused to LldR was measured by a photomultiplier tube (PMT)-based photometry system (Till Photonics GmbH). Regular pulses of indigo light (438 ± 12 nm) from a homemade LED-based monochromator excited the fluorescent proteins. Simultaneously, the emission, which passed through a 40×, NA 0.95 dry immersion objective lens (I×71; Olympus), was split into short (480 ± 40 nm) and long (535 ± 15 nm) wavelengths by a dichroic mirror (505DCLP) and band-pass filters (D480-40 for short wavelengths and ET535-30 for long wavelengths; Chroma Technology) and detected by two PMTs connected with an FDU-2 fluorescence detection unit (Till Photonics GmbH). The analog outputs were digitized by the data acquisition board (PCI-6221; National Instruments) at a sampling rate of 10 kHz and averaged. Then, FRETr was calculated by the following equation: $FRETr = (Venus_C - cFactor \times mTFP_C)/mTFP_C$.[42] The numerator is the voltage output of the long-wavelength PMT minus calculated bleed-through from the donor, indicating excitation of acceptor by FRET, and the denominator is the voltage output of the short-wavelength PMT, indicating direct donor excitation by the light source. The bleed-through from mTFP to the long-band PMT was 0.45, and from Venus to short-band PMT, it was 0.02, which was ignored. Timing control, data acquisition, and real-time calculation of FRETr, including background compensation, were performed using an in-house program that also controlled the monochromator through the data acquisition interface. To calculate ΔFRETr in a time series, the average of 5-s points before drug (glutamate or Aβ) treatment was set to the initial value. Solution exchange for drug treatment was accomplished by a theta tube moved laterally by a step-driven motor (SF-77C; Warner Instruments) and was completed within 20 ms. The raw data were processed with Excel 2016 (Microsoft).

Staining of live cell fluorescent organelle dyes

Intracellular lysosomes and mitochondria were stained as previously described.[43] Briefly, astrocytes were incubated with LysoTracker and MitoTracker (Thermo Fisher Scientific) in a final concentration (250 nM) for 30 min at 37°C. After removing dye-containing media, cells were washed with DPBS three times. Astrocytes were then fixed with 4% paraformaldehyde for 10 min and mounted on the coverslips with DAKO mounting media. Images were acquired with the LSM 800 confocal microscope immediately after fixation.

Filipin III staining

Astrocytes were fixed with 4% paraformaldehyde for 10 min and the cholesterol staining kit (BioVision) was used for filipin III staining as described previously.[17] Briefly, cells were washed with assay buffer and incubated with filipin III staining solution for 1 h at room temperature. Images were acquired with the LSM 800 confocal microscope immediately after washing and mounting.

Autophagy flux assay

Transient transfection of ptfLC3 (plasmid encoding mRFP-GFP-MAP1LC3B, Addgene #21074) was performed with Lipofectamine Stem Transfection Reagent (Invitrogen) by following the manufacturer's instruction. Transfected cells were fixed with 4% PFA after 24 h and imaged under the LSM 800 confocal microscope. The images were analyzed by quantifying the number of RFP puncta (autolysosome) and RFP/GFP colocalization puncta.

Lysosomal activity assay (cathepsin B)

The activity of cathepsin B in astrocytes was measured using a Fluorometric Assay kit (BioVision) according to the manufacturer's protocol. Briefly, cells were dissociated with TrypLE and lysed on ice for 10 min. Supernatants were incubated with cathepsin B substrates (Ac-RR-AFC) at 37°C for 2 h and excitation/emission wavelength (400/505 nm) was measured using a fluorescent microplate reader.

Time-of-flight secondary ion mass spectrometry (ToF-SIMS)

All the sample preparation procedures were performed as described previously.[43,44] After fixation with 10% formalin, cells were further fixed with 2% glutaraldehyde. Cells were washed twice with 150 mM ammonium acetate solution and then rinsed several times with distilled water. Then, cells were covered with graphene carefully and allowed to dry for 30 min. Using a plasma chamber (CUTE, Femto Science Inc.), air-plasma was treated to graphene-covered cells to remove graphene and organic impurities on the surface of samples at 1.1–1.3 Torr, 50 kHz, 100 W, and 70 sccm of air for 2 min. ToF-SIMS analysis was performed on a ToF-SIMS 5–100 instrument (ION-TOF) using a pulsed 30 keV $Bi3^+$ primary ion beam in the delayed extraction mode with a primary ion dose of 3×10^{12} ions/cm^2 for the positive ion ToF-SIMS images over a 500 × 500 μm^2 area with 256 × 256 pixels. Internal mass calibration for all the ToF-SIMS spectra was conducted using the peaks of CH_3^+, Na^+, $C_2H_3^+$, $C_3H_5^+$, and $C_{27}H_{45}^+$ for the positive mode before further analysis. We acquired ToF-SIMS positive ion images of fragmented cholesterol a $C_7H_{11}^+$ (*m/z* 95.10),

phosphocholine at $C_5H_{15}NPO_4^+$ (*m/z* 184.09), sphingomyelin at $C_{47}H_{94}N_2O_6P^+$ (*m/z* 86.13). The ion signal intensity was counted as the sum of the pixel number in the cropped area (207 × 207 μm^2 area with 106 × 106 pixels).

Electron microscopy

Astrocytes were fixed in 2.5% glutaraldehyde and 2% paraformaldehyde in 0.15 M Sodium Cacodylate buffer pH 7.4. for 2 h at room temperature. Cells were washed three times with 0.15 M Sodium Cacodylate buffer for 5 min, and post-fixation was performed with 2% osmium tetroxide for 1 h at room temperature. Following washing three times with DH_2O for 5 min, samples were dehydrated through ethanol series. Samples were infiltrated with ethanol:Epon812 (2:1) for 1 h at room temperature, then with ethanol:Epon812 (1:2) for 1hr. Samples were embedded with 100% Epon812 overnight at room temperature and were polymerized at 65°C the next day after two changes of fresh 100 resin for 1hr. Thin sections (60 nm) were placed on formvar-coated copper single slot grids (EMS) and stained with Lead citrate and Uranyl acetate. Sections were imaged with FEI Tecani G2 F20 TWIN TMP at 200 Kv accelerating voltage using Gatan TEM CCD camera at DGIST Hub of Ubiquitous Based intra-services.

Proteomics

Peptide generation via in-solution digestion

For in-solution digestion, cells were dissolved in 0.2% ProteaseMAX (Promega) in 40 mM ammonium bicarbonate (NH_4HCO_3). After sonication at 30% amplitude for 3 s on, 10 s off, 10 times, the cell lysates were 4-fold diluted with 40 mM ABC. After 20 min incubation with 10 mM dithiothreitol (DTT) at 56°C, 20 mM iodoacetamide (IAA) was added and incubated for 20 min at room temperature in the dark. After estimation of protein amounts by the BCA protein assay, a 1:50 ratio of trypsin Lys-C mixture (Promega) was added to 100 μg of protein for 4 h at 50°C. After centrifugation at 16,000 × g for 10 s at 4°C, the supernatant was collected. The cells were treated with 0.5% trifluoroacetic acid (Thermo Fisher Scientific) for 5 min at 25°C to stop the reaction. After drying, the peptides were applied to C18 spin column (Thermo Fisher Scientific) and the eluents were dried.

Mass analysis

The peptides were analyzed using a Q Exactive Plus Hybrid Quadrupole–Orbitrap Mass Spectrometer interfaced with an EASY-Spray source (Thermo Fisher Scientific). Chromatographic separation of peptides was achieved using an UltiMate 3000 RSLCnano system (Thermo Fisher Scientific), equipped with an Acclaim PepMap 100 C18 HPLC Column (75 μm × 2 cm, 3 μm nanoviper; Thermo Fisher Scientific) as the loading column and an EASY-Spray PepMap RSLC C18 Column (75 μm × 50 cm, 2 μm; Thermo Fisher Scientific) as the separation column. Peptides were loaded from the RS auto-sampler and separated with a linear gradient of acetonitrile (ACN)/water, containing 0.1% formic acid, at a flow rate of 300 nL/min. The liquid chromatography eluent was electrosprayed directly from the analytical column, and a voltage of 2.0 kV was applied via the liquid junction of the nanospray source. Peptide mixtures were separated with a gradient of 10–50% ACN for 80 min. The analysis method consisted of a full MS scan with a range of 350–2000 m/z and data-dependent MS/MS on the ten most intense ions from the full MS scan. The mass spectrometer was programmed to the data-dependent acquisition mode. Mass spectrometer calibration was performed using the proposed calibration solution, according to the manufacturer's instructions.

Database searching

To perform the database search, tandem mass spectra were processed using Proteome Discoverer software (Thermo Fisher Scientific) version 2.41. The spectral data were searched against the Human Uniprot database (release version 2022_06). All identified proteins had a false discovery rate of $\leq$1%, which was calculated at the peptide level. Search parameters allowed for a tryptic specificity of up to two missed cleavages, with methylthio-modifications of cysteine as a fixed modification and oxidation of methionine as a dynamic modification. The mass search parameters for +1, +2, and +3 ions included mass error tolerances of 20 ppm for precursor ions and 0.6 Da for fragment ions. To calculate quantitative changes in the identified proteins among experimental groups, we used LFQ analysis sequence of Proteome Discoverer.

Bioinformatics

DAVID bioinformatics resource 6.8 was used for GO-based function annotation. IPA was used for in-depth bioinformatics analysis. For the identified proteins, Uniprot protein accession numbers coupled with the value of normalized fold changes were uploaded to IPA in the protein expression criteria. We used the following criteria for quantitative pathway analysis: *Z* score cutoff = 0.5, –log (p value) > 1.3.

QUANTIFICATION AND STATISTICAL ANALYSIS

Prism 9 (GraphPad) was used for statistical analysis. Unpaired Student's t-test or one-way ANOVA test with Dunnett's post hoc analysis was used.